Targeting CCL2/CCR2 Signaling Overcomes MEK Inhibitor Resistance in Acute Myeloid Leukemia

Rucha V. Modak[1,2,3,4], Katia G. de Oliveira Rebola[1,2,3,4], John McClatchy[1,2,3,4], Mona Mohammadhosseini[1,2,3,4], Alisa Damnernsawad[2,4,5], Stephen E. Kurtz[1,2,4], Christopher A. Eide[1,2], Guanming Wu[6], Ted Laderas[6], Tamilla Nechiporuk[2,4], Marina A. Gritsenko[7], Joshua R. Hansen[7], Chelsea Hutchinson[7], Sara J.C. Gosline[7,8], Paul Piehowski[7], Daniel Bottomly[6], Nicholas Short[9], Karin Rodland[7], Shannon K. McWeeney[6], Jeffrey W. Tyner[2,4], and Anupriya Agarwal[1,2,3,4]

ABSTRACT

Purpose: Emerging evidence underscores the critical role of extrinsic factors within the microenvironment in protecting leukemia cells from therapeutic interventions, driving disease progression, and promoting drug resistance in acute myeloid leukemia (AML). This finding emphasizes the need for the identification of targeted therapies that inhibit intrinsic and extrinsic signaling to overcome drug resistance in AML.

Experimental Design: We performed a comprehensive analysis utilizing a cohort of ∼300 AML patient samples. This analysis encompassed the evaluation of secreted cytokines/growth factors, gene expression, and *ex vivo* drug sensitivity to small molecules. Our investigation pinpointed a notable association between elevated levels of CCL2 and diminished sensitivity to the MEK inhibitors (MEKi). We validated this association through loss-of-function and pharmacologic inhibition studies. Further, we deployed global phosphoproteomics and CRISPR/Cas9 screening to identify the mechanism of CCR2-mediated MEKi resistance in AML.

Results: Our multifaceted analysis unveiled that CCL2 activates multiple prosurvival pathways, including MAPK and cell-cycle regulation in MEKi-resistant cells. Employing combination strategies to simultaneously target these pathways heightened growth inhibition in AML cells. Both genetic and pharmacologic inhibition of CCR2 sensitized AML cells to trametinib, suppressing proliferation while enhancing apoptosis. These findings underscore a new role for CCL2 in MEKi resistance, offering combination therapies as an avenue to circumvent this resistance.

Conclusions: Our study demonstrates a compelling rationale for translating CCL2/CCR2 axis inhibitors in combination with MEK pathway-targeting therapies, as a potent strategy for combating drug resistance in AML. This approach has the potential to enhance the efficacy of treatments to improve AML patient outcomes.

Introduction

Acute myeloid leukemia (AML) is a highly aggressive hematologic malignancy with a significant impact on mortality. In the United States alone, there are approximately 20,000 new AML diagnoses and more than 10,000 estimated deaths from the disease annually (1, 2). A major challenge in AML treatment is the presence of genetic heterogeneity with a diverse mutation spectrum among patients (3–5). Although targeted therapies have shown some efficacy, including recent approvals of inhibitors such as gilteritinib as well as ivosidenib or enasidenib for patients harboring mutations in FLT3 or IDH1/2, respectively (6–8), single-agent targeted therapies have limited overall benefit due to the rapid emergence of resistance. Therefore, novel combination approaches are urgently needed to improve treatment outcomes (9). The combination of the BCL2 inhibitor venetoclax with a hypomethylating agent offered high initial response rates in newly diagnosed older patients with AML or those unfit for intensive chemotherapy regimens (10). However, the need for new strategies to target AML remains evident, particularly in relapsed/refractory cases.

Emerging evidence suggests that the bone marrow microenvironment, characterized by the secretion of cytokines, chemokines, and growth factors, plays a crucial role in leukemogenesis, disease progression, and drug resistance (11–13). For example, IL6 and CXCL12/stromal cell-derived factor 1 (SDF-1) have been shown to protect malignant cells in the bone marrow microenvironment from therapy (11–13). Similarly, FLT3 ligand and FGF2 have been implicated in promoting resistance to therapy in FLT3-mutated AML (14, 15). Further, the inhibition of IL1 signaling selectively suppresses the growth of AML cells (16–19). These findings highlight the importance of comprehensively evaluating the secreted factors within the AML microenvironment to develop combinatorial approaches targeting both intrinsic and extrinsic signals to reduce AML burden and overcome drug resistance.

[1]Division of Oncological Sciences, Oregon Health & Science University, Portland, Oregon. [2]Knight Cancer Institute, Oregon Health & Science University, Portland, Oregon. [3]Department of Molecular and Medical Genetics, Oregon Health & Science University, Portland, Oregon. [4]Department of Cell, Developmental, & Cancer Biology, Oregon Health & Science University, Portland, Oregon. [5]Department of Biology, Faculty of Science, Mahidol University, Bangkok, Thailand. [6]Division of Bioinformatics & Computational Biology, Oregon Health & Science University, Portland, Oregon. [7]Pacific Northwest National Laboratory, Richland, Washington. [8]Department of Biomedical Engineering, School of Medicine, Oregon Health & Science University, Portland, Oregon. [9]Department of Leukemia, MD Anderson Cancer Center, Houston, Texas.

R.V. Modak, K.G. de Oliveira Rebola, J. McClatchy, and M. Mohammadhosseini contributed equally to this article.

Corresponding Author: Anupriya Agarwal, Knight Cancer Institute, Oregon Health & Science University, 3181 SW Sam Jackson Park Road, Portland, OR 97239. E-mail: agarwala@ohsu.edu

Clin Cancer Res 2024;30:2245–59

doi: 10.1158/1078-0432.CCR-23-2654

Translational Relevance

Overcoming drug resistance in acute myeloid leukemia (AML) remains an unmet challenge in clinical practice. Our comprehensive analysis identified a pivotal translational avenue for combating this obstacle by targeting both extrinsic and intrinsic signaling. Specifically, we have demonstrated that increased levels of the chemokine CCL2 play a significant role in promoting resistance to MEK inhibition. Importantly, our findings suggest that combining MEK inhibitors with agents targeting the CCL2/CCR2 pathway holds great promise as a novel treatment approach to combat drug resistance in patients with AML. This translational relevance underscores the potential to translate our laboratory discoveries into tangible clinical benefits. Our large resource with 300 primary AML samples correlating microenvironment factors and gene expression with response to small molecules, can identify new drug response pathways in the context of microenvironment to design novel treatment options for preclinical and clinical testing and to improve AML outcomes.

In this study, we identified secreted factors in the AML microenvironment that modulate sensitivity to a panel of small molecules. Specifically, we focused on MEK inhibitor (MEKi) resistance, as mutations in MAPK pathways (NRAS, KRAS, PTPN11) are common in myeloid and lymphoid leukemias and activate MEK signaling pathways. However, MEKi, including trametinib have not been effective clinically due to the rapid development of resistance (20–22). We identified that monocyte chemoattractant protein-1 (MCP-1/CCL2) drives MEKi resistance. C–C motif chemokine ligand 2 (CCL2) is a chemotactic cytokine that attracts monocytes and retains tumor-activating macrophages (TAM) at the tumor site. CCL2 is thus associated with poor prognosis in various cancers including breast, lung, pancreatic, and prostate cancers (23–28). Elevated CCL2 levels have also been correlated with acute lymphoblastic leukemia (ALL) (29). We found that a high level of CCL2 leads to reduced sensitivity to the MEK1/2 inhibitor, trametinib. We demonstrate that blockade of CCL2/CCR2 signaling resensitizes leukemia cells to trametinib, suggesting a new potential combination treatment strategy to overcome MEKi resistance and improve outcomes in patients with AML. Moreover, the implications of our study extend beyond AML and have relevance for other cancers as well.

Materials and Methods

Primary patient samples

Primary samples from patients with AML were obtained from the Beat-AML cohort (5), following Oregon Health and Science University (OHSU) Institutional Review Board guidelines. Within Beat-AML biorepository, the patients consented using informed written consent, and all studies involving human subjects were conducted following the Declaration of Helsinki guidelines and the Belmont Report. Peripheral blood samples and bone marrow aspirates obtained from patients with AML were processed to obtain plasma and mononuclear cells (MNC). Primary cells were used immediately upon isolation. If frozen MNC derived from patients with AML were used, those were reconstituted overnight at 37°C and 5% CO_2 in Iscove Modified Dulbecco Medium (IMDM) supplemented with 20% heat-inactivated FBS, 2 mmol/L L-glutamine, 100 mol/L penicillin, 100 μg/mL streptomycin, and 10^{-4} M β-mercaptoethanol before use.

Data integration and pathway enrichment analysis

Cytokine levels from the Luminex assays were integrated with *ex vivo* drug sensitivity data and RNA-sequencing data for 299 AML patient samples using in-house developed R scripts. Samples falling into the top and bottom 20th percentiles of the AUC, which was used to measure drug response, were considered resistant and sensitive to a particular drug. The gene differential expression analysis between drug-sensitive and -resistant patient samples was conducted using the Limma package (30). The R scripts are available upon request. Lists of differentially expressed genes with FDR < 0.05 were subject to pathway enrichment analysis using Reactome pathways and the web-based pathway analysis tools. Significant pathways with FDR < 0.05 were collected for the hierarchical clustering analysis and the enrichment map plot using EnrichmentMap, a Cytoscape app (31).

AML cell lines

MOLM13 and OCI-AML2 cell lines were obtained from ATCC. Cell lines were thawed in RPMI1640 media supplemented with 20% FBS, 2 mmol/L L-glutamine, 100 U/mL penicillin, and 100 μg/mL streptomycin (R20) at 37°C and 5% CO_2 and then maintained in 10% FBS containing media. Cell lines were maintained at a density of 0.5 to 1 million cells per milliliter. The trametinib-resistant MOLM13 cell line was established by gradually increasing the concentration of trametinib starting from 10 nmol/L and replacing media twice a week over 12 weeks and then maintained in 50 nmol/L and further increased to 100 nmol/L trametinib. The OCI-AML2 cell line was established by increasing the concentration of trametinib starting from 1 nmol/L and replacing media twice a week over 12 weeks, maintained in 10 nmol/L trametinib. Similarly, trametinib-resistant AML cell lines with CCL2 were established in increasing concentrations of trametinib (10 nmol/L–1 μmol/L) over 14 weeks with or without 10 ng/mL CCL2 (Peprotech); media was replaced with fresh trametinib and CCL2 twice weekly. Once resistance was established, resistant cell lines were maintained in 100 nmol/L trametinib ± CCL2, and cell lines were not kept for more than 8 weeks between each thaw. Cell numbers were recorded weekly. All cell lines were confirmed mycoplasma-negative every month and prior to their experimental use. Cell line authentication was done via the short tandem repeat (STR) method by OHSU core facilities.

Cell line sequencing

Whole-exome sequencing was performed on MOLM13 cell lines cultured for the long term in trametinib only (T3) or MCP-1 and trametinib (TM1–TM4) cultures. DNA extraction was performed on each of the cell lines using Blood & Tissue Kit (Qiagen, Catalog No. 69504). Sequencing was carried out using 50 ng of genomic DNA using the Illumina Nextera RapidCapture Exome capture probes, which provide a coverage of 45 Mb of the genomic DNA-coding regions. Samples were run on the NovaSeq for 200 cycles. Variant allele frequencies (VAF) were analyzed using a standard pipeline (32).

Cytokine measurements

Cytokine levels in AML patient samples were measured from plasma (25 μL) using the MILLIPLEX MAP Human Cytokine/Chemokine Magnetic Bead Panel - Immunology Multiplex Assay (Millipore, Sigma, HCYTOMAG-60K) comprising 41 cytokines and growth factors as per the manufacturer's protocol. CCL2 levels from sensitive and trametinib-resistant MOLM13, and OCI-AML2 cell lines were determined using the Human CCL2 Quantikine ELISA Kit (Biotechne, DCP00). Cells were washed in PBS and plated at a concentration of 10^6 cells/mL in R20 medium for 24 hours. Conditioned

media was collected, concentrated using Amicon Ultra-4 Centrifugal Filter Unit (Millipore, Sigma), and measured as per the manufacturer's instructions. CCL2 levels were normalized to FBS medium only control and expressed as pg/mL.

Small-molecule inhibitor testing on primary AML samples

Ex vivo drug sensitivity assays on primary AML samples were conducted as described previously (33). Primary MNC cells were plated at a density of 10,000 cells per well in the presence of a seven-dose concentration series ranging from 0.014 to 10 μmol/L for trametinib (Selleck Chem) and cultured for 3 days followed by incubation with CCR2i RS540393 (MedChemExpress) with 0, 2.2, 6.6, and 20 μmol/L for 3 additional days. MTS colorimetric assay (AqueousOne, Promega) was used to determine the optical density of 490 nm as a measure of viability.

Small-molecule inhibitor testing using AML cell lines

Drug sensitivity assays on AML cell lines were conducted as described previously (33). AML cell lines were plated at a density of 1,250 cells per well in the presence of seven-dose concentration series ranging from 0.014 to 10 μmol/L for trametinib (Selleck Chem) in combination with either 0.028 to 20 μmol/L for RS504393 (MedChemExpress), 0.014 to 10 μmol/L for JNKi SP600125 (MedChemExpress), 0.014 to 10 μmol/L for dasatinib (MedChemExpress), 0.014 to 10 μmol/L for idelalisib (MedChemExpress), or 0.014 to 10 μmol/L for palbociclib (MedChemExpress) and cultured for 72 hours. MTS colorimetric assay (AqueousOne, Promega) was used to determine the optical density of 490 nm as a measure of viability. The free web application SynergyFinder was used for drug–interaction analysis and multidrug combination response data visualization (34).

Phosphoproteomics sample preparation

MOLM-13 parental (sensitive) and trametinib-resistant cell lines were maintained for 18 hours in starvation medium (0.1% BSA in RPMI, with 2 mmol/L L-glutamine, and 100 U/mL penicillin, and 100 μg/mL streptomycin). Starved MOLM-13 sensitive cells were treated with trametinib for 3 hours prior to treatment with 10 ng/mL CCL2 for the indicated time. MOLM-13 resistant lines were maintained in the presence of 50 nmol/L trametinib over the 18-hour starvation period and treated with 10 ng/mL CCL2 for the indicated time. At least 15 million cells were used per condition, and cell pellets were harvested and washed twice with ice-cold PBS to remove all the FBS and used for phosphoproteomic analysis.

Protein extraction and digestion

Sample preparation protocols for proteomics was based on the protocol developed under the Clinical Proteomic Tumor Analysis Consortium (CPTAC). Cell pellets were lysed using fresh lysis buffer containing 8 M urea (Sigma-Aldrich Inc.), 50 mmol/L Tris pH 8.0, 75 mmol/L sodium chloride, 1 mmol/L ethylenediamine tetra-acetic acid, 2 μg/mL Aprotinin (Sigma-Aldrich Inc.), 10 μg/mL Leupeptin (Roche), 1 mmol/L PMSF in EtOH, 10 mmol/L sodium fluoride, 1% of phosphatase inhibitor cocktail 2 and 3 (Sigma-Aldrich Inc.), 20 μmol/L PUGNAc, and 0.01 U/μL Benzonase. After adding 500 μL of chilled lysis buffer, the samples were vortexed for 10 seconds and then placed in a thermomixer set for 15 minutes at 4°C and 800 rpm. The lysis step was repeated by vortexing samples for an additional 10 seconds, followed by a second 15-minute incubation. The samples were then centrifuged for 10 minutes at 4°C and 18,000 rcf to remove cell debris. Following centrifugation, the protein supernatant was transferred to a fresh tube. A BCA assay (Thermo Fisher Scientific Inc.) was performed on the supernatant to determine protein yield.

Protein concentrations were normalized before the sample was reduced with 5 mmol/L dithiothreitol (DTT; Sigma-Aldrich Inc.) for 1 hour at 37°C and 800 rpm. Reduced cysteines were alkylated with 10 mmol/L iodoacetamide (Sigma-Aldrich Inc.) for 45 minutes at 25°C and 800 rpm in the dark. The sample was diluted fourfold with 50 mmol/L Tris HCl pH 8.0, and Lys-C (Wako Chemicals) was added at a 1:20 enzyme:substrate ratio, followed by an incubation for 2 hours at 25°C, shaking at 800 rpm. Trypsin (Promega) was then added at a 1:20 enzyme:substrate ratio, followed by a 14-hour incubation set at 25°C and 800 rpm. The sample was quenched by adding formic acid (FA) to 1% and centrifuged for 15 minutes at 1,500 rcf to remove any remaining cell debris. The peptides were desalted using a C18 solid-phase extraction (SPE) cartridge (Waters Sep-Pak).

TMT labeling

After drying down SPE eluent by vacuum centrifugation, each sample was reconstituted with 50 mmol/L HEPES, pH 8.5 to a concentration of 5 μg/μL. Treatment conditions were evenly distributed across TMT plexes using a randomized-block study design. Each 0.8 mg isobaric tag aliquot was dissolved in 40-μL anhydrous acetonitrile to a final concentration of 20 μg/μL. The tag was added to the sample at a 1:1 peptide:label ratio and incubated in a thermomixer for 1 hour at 25°C and 400 rpm, then diluted to 2.5 mg/mL with 50 mmol/L HEPES pH 8.5, 20% acetonitrile (ACN). Finally, the reaction was quenched with 5% hydroxylamine and incubated for 15 minutes at 25°C and 400 rpm. The samples were then combined per each plex set and concentrated in a speed-vac before a final C18 SPE cleanup. Each 11-plex experiment was fractionated into 96 fractions by high pH reversed-phase separation, followed by concatenation into 12 global fractions for MS analysis.

Peptide fractionation by basic reversed-phase LC

The experiment was performed as described previously (35). In brief, the peptides were further fractionated using a reversed-phase Waters XBridge C18 column (250-mm × 4.6-mm column packed with 3.5 μmol/L particles) on Agilent 1200 HPLC System (solvent A: 5 mmol/L ammonium formate, pH 10, 2% ACN and solvent B: 5 mmol/L ammonium formate, pH 10, 90% ACN) operating at a flow rate of 1 mL/min. Peptides were separated by a gradient mixture from 0% B to 16% B in 6 minutes, 40% B in 60 minutes, 44% B in 4 minutes, and ramped to 60% B in 5 minutes. The 60% B mixture was kept for 14 minutes. Fractions were collected from at 2 to 95 minutes during the fractionation run, and a total of 96 fractions was collected at equal time intervals. These 96 fractions were subsequently concatenated into 12 fractions for global proteome and six fractions for phosphoproteome analysis. Each pooled fraction was dried down by vacuum centrifugation.

Phosphopeptide enrichment

The procedure for phosphopeptide enrichment by Immobilized Metal Affinity Chromatography (IMAC) was performed as described previously (36). Briefly, the IMAC tip was inserted into a 96-well tip holder. Fifty millimoles per liter EDTA in 1 M NaCl was first used to remove Ni^{2+} ions (1,000 g, 1 minute). The tip was then activated with 100 mmol/L $FeCl_3$ (1,000 g, 1 minute) and equilibrated with 1% (v/v) acetic acid (1,000 g, 1 minute) at pH 3.0, prior to sample loading. For IMAC-C18 workflow, tryptic peptides were dissolved in 0.1% (v/v) TFA, 80% ACN, and loaded onto the IMAC tip (1,000 g, 1 minute). Then, the IMAC tips were washed by using 1% (v/v) TFA, 80% ACN

(1,000 g, 1 minute), and 1% (v/v) acetic acid (1,000 g, 1 minute), respectively. The IMAC tip was then inserted into activated desalting C18 StageTip. The bound phosphopeptides were eluted by 200 mmol/L $NH_4H_2PO_4$ (1,000 g, 3 minutes) onto the activated desalting C18 StageTip for desalting and directly eluted to sample vials of LC/MS, then dried under vacuum.

LC/MS-MS analysis

Lyophilized global and phosphorylated peptides were reconstituted in 0.1% FA with 2% ACN and 0.1% TFA with 2% ACN, respectively. The peptides were further analyzed by LC/MS-MS using a Q Exactive HF Hybrid Quadrupole-Orbitrap Mass Spectrometer (Thermo Fisher Scientific) connected to a nanoACQUITY UPLC system (Waters Corp.; buffer A: 0.1% FA with 3% ACN and buffer B: 0.1% FA in 90% ACN) as described previously (37). Peptides were separated by a gradient mixture with an analytical column (75 μmol/L i.d. × 20 cm) packed using 1.9-μmol/L ReproSil C18 and with a column heater set at 50°C. Peptides were separated by a gradient mixture: 2% to 6% buffer B in 1 minute, 6% to 30% buffer B in 84 minutes, 30% to 60% buffer B in 9 minutes, 60% to 90% buffer B in 1 minute, and finally 90% buffer B for 5 minutes at 200 nL/min. MS Spectra were collected from 350 to 1,800 *m/z* at a mass resolution setting of 60,000. A top 16 method was used for the collection of MS^2 spectra at a mass resolution of 30K. An isolation window of 0.7 *m/z* was used for higher-energy collision dissociation (HCD), singly charged species were excluded, and the dynamic exclusion window was 45 seconds.

TMT phosphoproteomics data processing

IMAC-enriched fraction datasets were searched as described above with the addition of a dynamic phosphorylation (+79.9663 Da) modification on Ser, Thr, or Tyr residues. The phosphoproteomic data were further processed with the Ascore algorithm (38) for phosphorylation site localization, and the top-scoring assignments were reported. To account for sample loading biases in the phosphoproteome analysis, we applied the same correction factors derived from the median-centering of the global proteomic dataset for normalization.

CRISPR/cas9 re-sensitization screen

Trametinib-resistant MOLM13 cells (TM1) were cultured in RPMI1640 media, supplemented with 20% FBS, 2 mmol/L L-glutamine, 100 U/mL penicillin, 100 μg/mL streptomycin, and fungizone. One million cells were transduced with Cas9 Blast+ virus and selected in blasticidin for 5 days. The Cas9+ cells were expanded to over 100 million and were infected with whole-genome CRISPR library (Addgene, No. 67989; ref. 39) at an MOI of 0.3. Cells were selected with puromycin for stable integration for 5 days. After selection, cells were cultured in 10 ng/mL CCL2 ligand during expansion until the collection time point(s). Five million cells were collected for the initial assessment (day 0) of library representation, and the rest were grown to 120 million and divided into duplicate flasks for each condition: DMSO only or Trametinib (100 nmol/L). At 14 days posttreatment initiation, cells were collected at 30 million or maximum, if less than 30 million (day 14). DNA was extracted by desalting and ethanol precipitation. For the DNA amplification and barcoding, 50 μg of DNA for each condition and 1 μg of library plasmid were amplified in a single PCR reaction using Herculase II (Agilent) enzyme. The primers contained a unique barcode identifying each sample, a library-specific sequence surrounding the guide RNA cloning site and adapters for next-generation sequencing (NGS) as described previously (39–41). The resulting PCR amplicons were resolved on 2% agarose gels, eluted, and purified using Amp-pure beads. Purified fragments were analyzed using QIAxcel (Qiagen) for purity and molarity, quantified and sequenced using NovaSeq 6000 (Illumina). Primer sequences are available upon request.

Generated reads were trimmed based on the presence of the known 3′ and 5′ flanking sequences (40) using Cutadapt (v2.3; ref. 42). A custom sgRNA sequence library was formed based on the Y. Kosuke library (Addgene, No. 67989). Alignments of each trimmed read to the custom library was performed using Bowtie2 (v2.3.5.1; ref. 43), the reads were subsequently filtered to only unique matches with no mismatches using Bamtools (v2.5.1; ref. 44). Counts per sgRNA were generated using MAGeCK (v0.5.8; Li, 2014). The set of sgRNA was filtered for low representation (those not seen in the plasmid or those with ≤100 counts per million in more than half the samples) and then were normalized using Trimmed Mean of M (TMM; ref. 45). The edgeR package (v3.40.2; ref. 46) was used for each linear model, generating log2-fold changes and two-sided *P* values per sgRNA. FDR adjustment was performed using the *q* value approach (v2.30.0; ref. 47). Genes were prioritized by examining three separate approaches. First, we summarized each gene by its mid sgRNA *P* value. This is done by ranking guides by their *P* value and choosing the "middle" sgRNA as a representative. Next, we evaluated significance by employing a statistical method called Camera (48). This method compares the average log2-fold change of sgRNA within a particular gene with those assigned to other genes. We determined significance using both *P* values and FDR/q values. Finally, we assessed concordance in terms of significance and log2-fold change using the Tiering approach we developed previously (40). There are five levels of tiers (tiers 1, 2, 3, singletons, and unassigned), where Tier1 genes show the highest concordance, singletons only have one significant sgRNA, and unassigned genes do not meet the fold-change criteria. Raw data files are accessible at GEO accession (GSE235183).

Immunoblot analysis

Cell lysates for immunoblotting were prepared as described previously (16). Proteins were run on 4% to 12% Bis-Tris gels, and immunoblots were probed with CCL2 mAb (clone 2D8; Thermo Fisher Scientific; MA5–17040) and CCR2 (clone D14H7; Cell Signaling Technologies, No. 12199). Expression was normalized using actin or GAPDH (Thermo Fisher Scientific, AM4300) or vinculin (Cell Signaling Technologies, No. 13901) using densitometric analysis from ImageLab software and represented as fold change with respect to trametinib sensitive (respective parental cells). When indicated, cell lines were cultured for 16 hours in a starvation medium (0.1% BSA in RPMI supplemented with 2 mmol/L L-glutamine and 100 U/mL penicillin, and 100 μg/mL streptomycin) in the presence of trametinib. Cell lines were stimulated with 10 ng/mL CCL2 and whole cell lysates were analyzed by immunoblotting for detection of phospho-MEK1/2 (Ser221; Cell Signaling Technologies, No. 2338), phospho-ERK1/2 (Thr202/Tyr204; Cell Signaling Technologies, No. 4377), phospho-JNK1/JNK2 (Thr183/Tyr185; Thermo Fisher Scientific, No. 700031), phospho-SRC (Ser17; Cell Signalling Technologies, No. 12432), phospho-Rb (Ser780; Cell Signaling Technologies, No. 8180), phospho-P70 S6 (Thr421/Ser424; Cell Signaling Technologies, No. 9204), phospho-PI3 Kinase p85 (Tyr458)/p55 (Tyr199; Cell Signaling Technologies, No. 17366), phospho-STAT5 (Tyr694; Cell Signaling Technologies, No. 9314), and phospho-AKT (Ser473; Cell Signaling Technologies, No. 4058). The phosphoprotein levels were normalized to the respective total protein using densitometric analysis from ImageLab software. β-Actin (13E5; Cell Signaling Technologies, No. 4970), GAPDH (14C10; Cell Signaling Technologies, No. 2118) or Vinculin (E1E9V; Cell Signaling Technologies, No. 13901) were used as protein loading controls.

Lentiviral transduction

Short-hairpin RNA (shRNA) targeting human CCR2 were purchased from OriGene Technologies (Catalog No. TL321181). The plasmids were amplified and packaged for transduction using VSV-G envelope plasmid (Invitrogen) and psPAX2 packaging plasmid (Addgene, No. 12260) by transfection in HEK 293T cells. Resistant cell lines were infected with the concentrated virus and selected using puromycin (1 μg/mL) to ensure stable integration of shRNA.

Flow cytometry for cell proliferation and apoptosis

Cells cultured with either trametinib, RS504393, or a combination of both were stained by suspending a cellular concentration (1 million/mL) with Cell Trace Violet 5 μmol/L (Invitrogen) on day zero, quenched with FBS, washed, and incubated for 3 days. Cells were stained with Annexin V for 15 minutes, rinsed, and suspended in 7-AAD (Annexin V Detection Kit; eBioscience) incubated for 30 minutes and acquired on the BD Symphony A5. Data were analyzed using FlowJo version 10.

Statistical analysis

Drug sensitivity data for cell lines and patient samples were represented in the form of percentage viability across a concentration range and fit a nonlinear regression. The statistical analyses used for the specific figures are indicated. In all cases, P value < 0.05 was considered significant denoted by * for $P < 0.05$, ** for $P < 0.01$, and *** for $P < 0.001$.

Data and materials availability

CRISPR data are accessible at GEO accession (GSE235183). Additional data are provided in the Supplementary tables. The reagents and additional details used in this study will also be shared upon requests made to agarwala@ohsu.edu.

Results

Distinct cytokines and signaling pathways are associated with specific drug responses in AML

To gain a comprehensive view of the extrinsic factors and signaling pathways that modulate drug response in AML, we quantified the levels of 41 secreted cytokines and chemokines in plasma samples from nearly 300 patients with AML (Supplementary Table S1). Cytokine levels were then compared with matched *ex vivo* sensitivity of primary mononuclear cells from these same patients to inhibitors of four major therapeutic targets that cover broad genetic subtypes and responses in AML: FLT3 (sorafenib), BCL2 (venetoclax), JAK (ruxolitinib), MEK (trametinib, selumetinib, and CI-1040; **Fig. 1A** and **B**). Samples with the lowest and highest 20% AUC values for *ex vivo* dose response were classified as sensitive and resistant, respectively for each drug as described previously (5). We identified that TNFα, IL1RA, MIP-1a, and IL8 were elevated in the sorafenib-resistant patient samples (P values of 0.0056, 0.04, 0.013, and 0.016, respectively). Higher levels of IL4 ($P = 0.021$), TGFα ($P = 0.044$), GRO ($P = 0.0093$), and CCL2 (P = 4.98E-7) were observed in trametinib-resistant AML samples. Notably, increased levels of CCL2 were likewise observed in AML patient samples that exhibited resistance to additional MEKi selumetinib ($P <$ 4.86E−6), CI-1040 ($P <$ 4.94E−5), and the JAK inhibitor ruxolitinib ($P = 0.0036$). In contrast, levels of CCL2 were significantly decreased in samples with venetoclax resistance ($P <$ 5.19E−4; **Fig. 1C** and **D**; Supplementary Table S2).

Because CCL2 levels were strongly associated with differential sensitivity to various drugs, we further investigated the potential causative role of CCL2 in modulating drug response. We treated mononuclear cells derived from patients with AML *ex vivo* with a concentration gradient of trametinib, ruxolitinib, or venetoclax in the presence of CCL2 for 72 hours and assessed viability. Primary AML cells showed increased resistance to trametinib and ruxolitinib in the presence of CCL2 as represented by significantly increased AUC values ($P < 0.020$ and 0.036, respectively), whereas sensitivity to venetoclax was enhanced ($P < 0.034$, **Fig. 1E**). Together, these findings indicate that specific secreted factors, such as CCL2, are associated with specific patterns of drug sensitivity.

High CCL2 levels are associated with trametinib resistance in primary AML cells and cell lines

Previous studies have reported increased levels of CCL2 in patients with leukemia (29, 49) and demonstrated a role of CCL2 in the migration of AML cells (50–53). However, the role of CCL2 in therapeutic resistance in AML remains unexplored. As the strongest association between plasma CCL2 levels and *ex vivo* drug sensitivity was observed for MEKi, we focused on identifying the role of CCL2 in resistance to MEKi. Differential gene expression analysis from RNA sequencing of the cohort of primary AML patient samples screened above identified that *ex vivo* response to trametinib was associated with increased enrichment of immune pathways including cytokine and interleukin signaling (Supplementary Figs. S1A–S1C; Supplementary Table S3). We also correlated trametinib *ex vivo* AUC sensitivity with clinical, cytogenetic, and mutation features for 208 AML samples (Supplementary Tables S4 and S5). Consistent with the above analysis (**Fig. 1C**), we found that increased plasma concentration of CCL2 correlated with decreased sensitivity to trametinib. We found trametinib sensitivity was also associated with the presence of NRAS mutations, CBFB-MYH11 translocation, and increased percentage of monocytes in peripheral blood, whereas decreased sensitivity was associated with older patients. (Supplementary Fig. S1D; Supplementary Table S4). Of these features, NRAS mutations, CBFB–MYH11 fusion, and increased monocytes showed trends for decreased levels of CCL2 in plasma (P values: 0.054, 0.029, and 9.84E−5, respectively) and increased sensitivity to trametinib.

To test whether high CCL2 levels are associated with resistance to MEK inhibition in AML, we generated trametinib-resistant AML cell lines by culturing MOLM13 and OCI-AML2 cells in an increasing concentration of trametinib and maintained in trametinib after establishment of resistance (**Fig. 2A**). Trametinib-resistant MOLM13 and OCI-AML2 were up to two- to threefold less sensitive to trametinib as determined by the AUC (**Fig. 2B**) and exhibited resistance to various MEK1 inhibitors respective to sensitive cells (Supplementary Fig. S2A). Withdrawal of trametinib for 2 weeks did not increase sensitivity to trametinib (Supplementary Fig. S2B). Both the trametinib-resistant cell lines showed an increase in the intracellular CCL2 protein levels in comparison with sensitive cells as measured by immunoblot analysis (**Fig. 2C**). Accordingly, secreted CCL2 levels measured by ELISA were ∼21.5- and ∼228.6-fold higher in conditioned media from trametinib-resistant cells compared with the respective sensitive (parental) cells (**Fig. 2D**).

To determine the direct contribution of trametinib to CCL2 levels, we treated sensitive AML cells with trametinib and found increased CCL2 production by ELISA. In contrast, withdrawal of trametinib from resistant cells did not reduce CCL2 levels, suggesting that trametinib-driven stress is sufficient to increase CCL2 production, and resistant cells likely maintain elevated CCL2 levels through genetic, transcriptomic, or additional molecular mechanisms (Supplementary Fig. S2C). To study the effect of CCL2 on sensitivity to

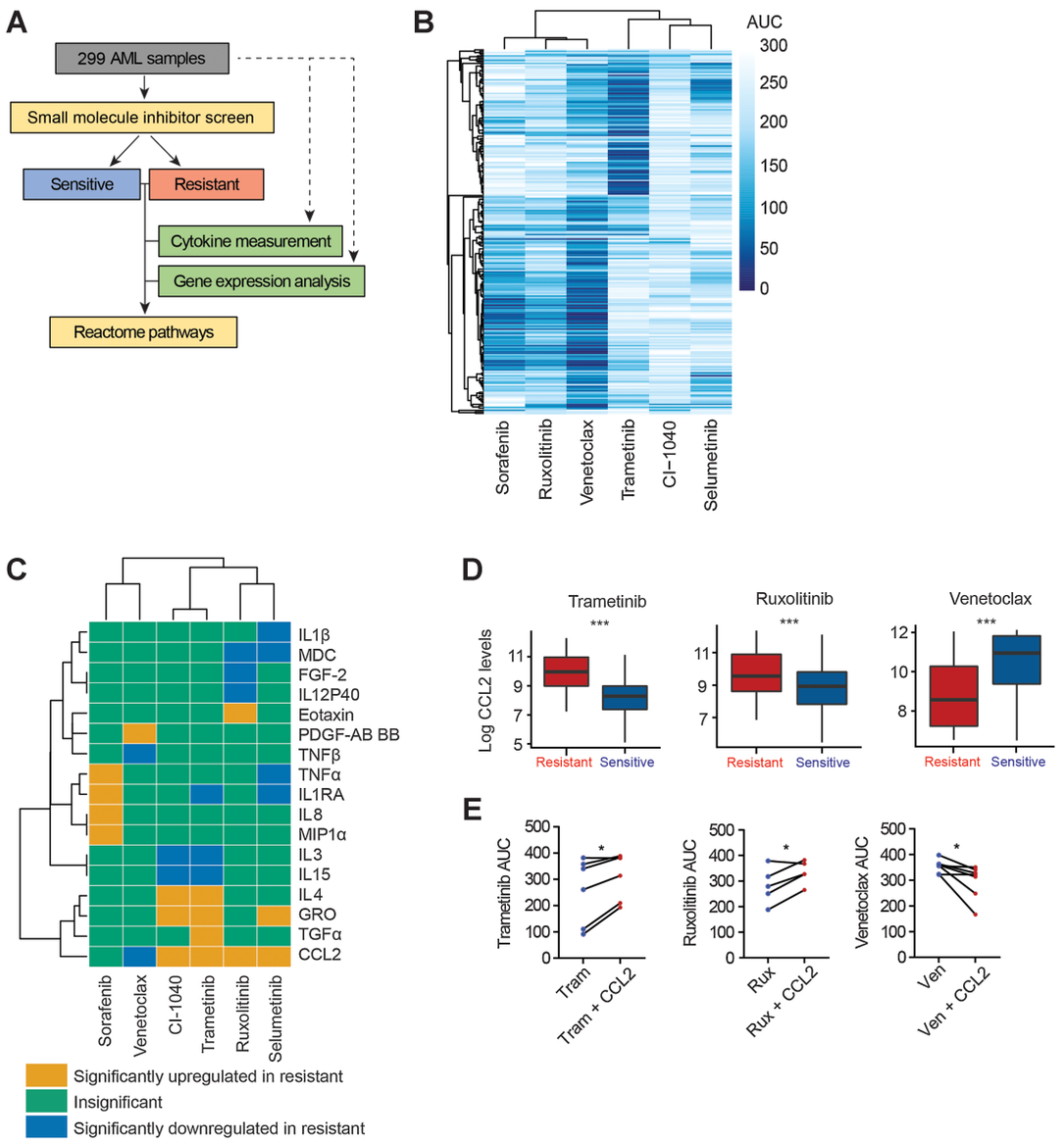

Figure 1.

Distinct cytokines and signaling pathways are associated with drug responses in AML. **A,** Representation of the data integration approach from 299 primary AML samples. Secreted cytokine levels using plasma derived from 299 AML patient samples, and the Beat AML database was leveraged for the *ex vivo* drug sensitivity and gene expression analysis for the matched samples. The drug screening data were classified as sensitive or resistant based on AUC for each drug and were integrated with the cytokine, RNA-seq, and Reactome pathway analysis. **B,** Hierarchical clustering of AUC for the indicated inhibitors for the 299 AML samples. **C,** Heat map constructed by integrating the cytokine expression data with *ex vivo* sensitivity profile of the inhibitors. Statistical significance was determined by *t* test with *P* value <0.05 as significant. **D,** CCL2 protein levels for AML patient samples sensitive and resistant to trametinib, ruxolitinib, and venetoclax from **Fig. 1C**. The measured abundance of CCL2 was log2-transformed in the plot. **E,** *Ex vivo* drug response of primary AML cells treated with the indicated inhibitors on a concentration gradient with or without 10 ng/mL CCL2 for 72 hours. Viability was determined by the MTS assay cell viability assay, and the results are represented as the AUC of individual samples (trametinib:Tram = 6, ruxolitinib: Rux *n* = 5, venetoclax: Ven *n* = 7). Statistical significance was determined by the two-tailed paired Student *t* test. *, $P \leq 0.05$ and ***, $P \leq 0.001$.

trametinib in AML cells, we cultured MOLM13 AML cells with an increasing concentration of trametinib over time with or without CCL2 for 14 weeks. In the cultures treated with trametinib only, two of the four replicates survived after 14 weeks. Although all four replicates treated with CCL2 and trametinib, expanded significantly (fourfold) compared with trametinib-only treated cultures over the 14-week culture period, suggesting CCL2 provides a growth and survival advantage for the emergence of trametinib-resistant cells at an early stage (**Fig. 2E**). In all cases, cell lines that grew out under treatment with trametinib or trametinib plus CCL2 were confirmed to confer resistance to trametinib and maintained MEK1 (MAP2K1) mutations at a VAF of ∼50% suggesting a uniformly heterozygous cell population similar to prior study (54) (**Fig. 2F**; Supplementary Table S6).

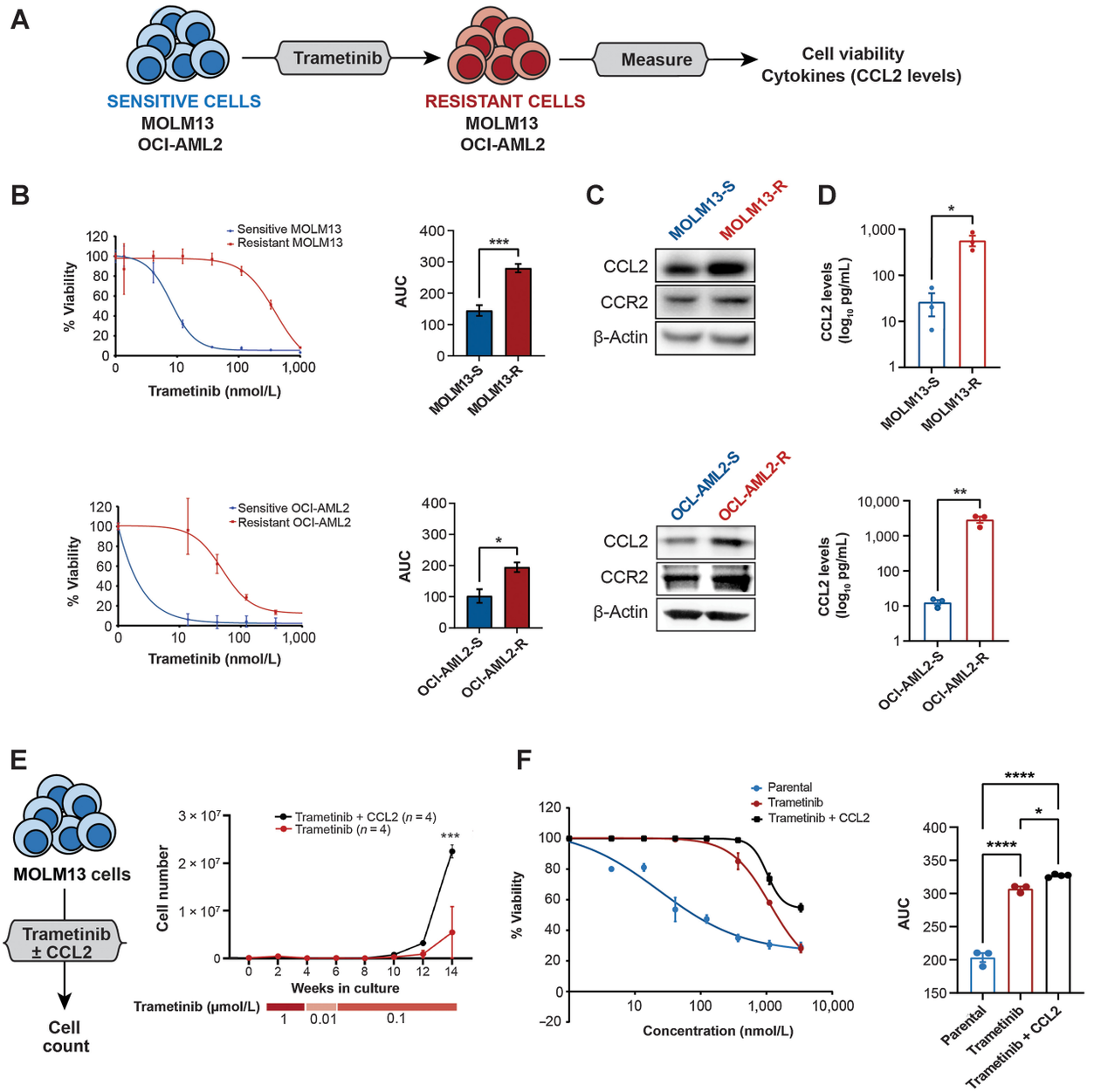

Figure 2.

Increased CCL2 levels are associated with trametinib resistance in AML. **A,** The generation of trametinib-resistant MOLM13 and OCI-AML2 cell lines. These AML cell lines were made resistant to trametinib by culturing the cells in gradually increasing concentrations of trametinib starting over 12 weeks as described in methods and maintained in trametinib by replacing media twice weekly. **B,** Viability of trametinib-sensitive (S) and -resistant (R) MOLM13 and OCI-AML2 cells across the indicated concentrations of trametinib as measured by colorimetric cell viability (MTS) assay (left) and their AUC (right). The data are shown as mean ± SEM from three technical replicates, representative of at least three independent experiments. Significance is determined using two-tailed Student *t* test. **C,** Representative immunoblots from trametinib-sensitive (S) and -resistant (R) MOLM13 and OCI-AML2 cells probed for CCL2 and CCR2. β-Actin was used as a loading control. **D,** Levels of CCL2 from the supernatant of sensitive and resistant MOLM13 and OCI-AML2 cells are shown as a log10 scale expressed as pg/mL. Mean values from three independent experiments are shown with significance calculated by the unpaired two-tailed Student *t* test. **E,** MOLM13 trametinib-sensitive AML cell lines cultured with trametinib (0.01–1 μmol/L) ± CCL2 (10 ng/mL) for 14 weeks ($n = 4$). The media was replaced with fresh trametinib and CCL2 twice weekly. Once resistance was established, resistant cell lines were maintained in 100 nmol/L trametinib ± CCL2. Total viable cell numbers over 14 weeks in culture are represented. Significance was determined using the two-way ANOVA. **F,** Cell viability of trametinib-sensitive (parental) and -resistant MOLM13 cells cultured ± CCL2 from **Fig. 2E** treated with the indicated concentrations of trametinib as measured using the MTS assay (left) and AUC (right). The data are shown as mean ± SEM from three technical replicates; representative of three independent experiments; significance determined by the one-way ANOVA. *, $P \leq 0.05$; **, $P \leq 0.01$; ***, $P \leq 0.001$; ****, $P \leq 0.0001$.

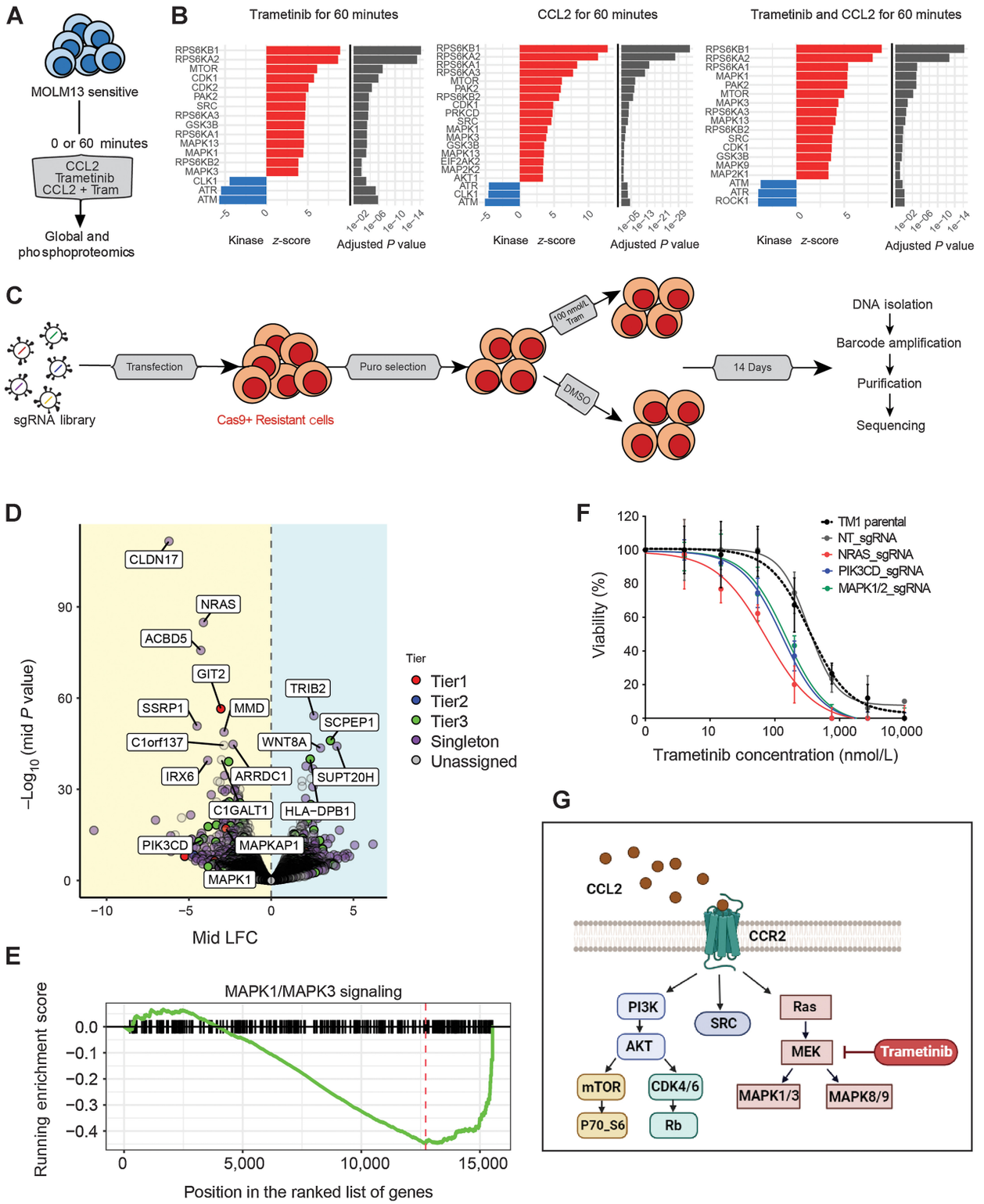

Figure. 3.

CCL2 or trametinib exposure activated prosurvival pathways in parental and trametinib-resistant AML cells. **A,** MOLM13 parental cells and treatment conditions used for phospho- and global proteomics. **B,** Kinase-substrate enrichment analysis (KSEA) of the enriched substrates for indicated kinases ($P < 0.05$) from the AML cells upon 60 minutes of trametinib, CCL2, or combination treatments. (*Continued on the following page.*)

CCL2 stimulation or MEK inhibition activates prosurvival pathways in AML cells

To evaluate the downstream changes conferred by CCL2 in the presence of trametinib, we performed global proteomics analysis of MOLM13 cells treated with trametinib alone or in combination with CCL2 (**Fig. 3A**). Similar to RNA-sequencing analysis of trametinib-resistant primary AML cells (Supplementary Fig. S1A), gene set enrichment analysis (GSEA) of the global proteomics data identified enrichment of several immunologic pathways in trametinib-resistant cell lines compared with trametinib-sensitive cells, as well as upregulation of cell cycle and protein synthesis pathways in the cells cultured with CCL2 and trametinib as compared to trametinib alone (Supplementary Fig. S3A). Because phosphorylation of proteins modulates multiple cellular processes, kinase-substrate enrichment analysis (KSEA) was used to infer changes in the activity of kinases by evaluating changes in the phosphorylation levels of their respective substrates (55, 56). KSEA of global phosphoproteomics revealed that combined treatment with trametinib and CCL2 for 60 minutes increased the activity of MAPK (MAPK1, MAPK3, MAPK9) and MTOR (MTOR, RPS6) pathways relative to trametinib-sensitive vehicle-treated cells and revealed increased activation of kinases involved in cell cycle progression or apoptosis (CDK1, PAK2). We also detected elevated phosphorylation of substrates for SRC and a trend for elevation of substrates of AKT1 (**Fig. 3B**; Supplementary Table S7; Supplementary Fig. S3B). Trametinib or CCL2 as a single agent induced similar changes in MAPK, mTOR, CDK, SRC, and JAK kinases, suggesting trametinib exposure may activate CCL2-dependent downstream signaling. Similarly, global proteomics analysis of resistant MOLM13 cells generated from long-term culture with trametinib with or without CCL2 indicated increased expression levels of MAPK, SRC, mTOR, and CDK kinases in the resistant in comparison to parental MOLM13 cells (Supplementary Fig. S3C; Supplementary Table S8). We validated these activated pathways by performing immunoblot analysis of CCL2-stimulated trametinib-resistant MOLM13 cells (Supplementary Fig. S3D).

As a complementary approach, we performed a genome-wide CRISPR-Cas9 re-sensitization screen to identify genes and pathways conferring resistance to trametinib. We transduced Cas9+ MOLM13 cells cultured long term with trametinib and CCL2, with a genome-wide CRISPR library targeting over 18,000 genes (39) (**Fig. 3C**) to identify loss-of-function genes that may lead to re-sensitization to trametinib. Comparison of depleted sgRNA hits between DMSO and trametinib-treated cells identified regulators of the MAPK/PI3K/RAS pathways, including *NRAS, PIK3CD,* and *MAPK* (**Fig. 3D** and **E**; Supplementary Table S9). To gain an insight into the global trametinib-dependent changes, we performed a GSEA analysis using the depleted sgRNA in the trametinib-treated group compared with DMSO-control group. Our data corroborated the involvement of multiple MAPK pathways (Supplementary Fig. S3E; Supplementary Table S10) as observed in proteomics analysis (**Fig. 3B**). To validate our CRISPR screening results, we transduced trametinib-resistant (TM1) MOLM13 cells with sgRNA targeting *NRAS, PIK3CD*, and *MAPK1/2* or a nontargeting sgRNA. The knockout lines showed increased sensitivity to trametinib in comparison with the nontargeting (NT) controls (**Fig. 3F**). Together, our CRISPR and proteomics analyses suggested trametinib resistance can be mediated by increased activation of prosurvival (PI3K/AKT/MAPK/mTOR) and cell-cycle pathways (**Fig. 3G**).

Targeting prosurvival and cell-cycle pathways downstream of CCL2 overcomes MEKi resistance

Both proteomics and CRISPR screening revealed a dependency of trametinib-resistant AML cells on several interregulated signaling pathways including SRC, PI3K/AKT/mTOR, MAPK, and CDK. To further prioritize which of these pathways may overcome drug resistance mediated by CCL2, we first interrogated *ex vivo* drug sensitivities in the Beat-AML database of primary AML samples and found that combination treatments targeting SRC (dasatinib), PI3K/AKT (idelalisib), mTOR (rapamycin), or CDK4/6 (palbociclib) with trametinib demonstrated significantly greater *ex vivo* sensitivity compared with respective single-agent treatment (all FDR-adjusted P values <0.001; **Fig. 4A** and **B**). However, no substantial improvement in sensitivity was observed for trametinib in combination with JQ1, a BET domain inhibitor (57) (**Fig. 4A** and **B**), confirming that the enhanced efficacy of these combinations is not just a cytotoxic effect of combining any second drug with trametinib. Interestingly, most of the RAS-mutated (NRAS or KRAS) AML samples maintained sensitivity to pan-MEKi such as CI1040, selumetinib, and trametinib (Supplementary Fig. S4A). In addition, trametinib-resistant RAS-mutated samples, selected with higher AUC (Supplementary Fig. S4A), can be further sensitized to combination treatments targeting PI3K/AKT (idelalisib) or CDK4/6 (palbociclib; Supplementary Fig. S4B).

Further, we validated these combinations in trametinib-resistant MOLM13 AML cell lines by analyzing drug–response curves and downstream signaling following the combination treatment of trametinib with idelalisib, dasatinib, or palbociclib. In addition, we included JNKi to inhibit MAPK signaling that has high activity in our proteomics analysis for trametinib-resistant samples. Our data indicated that the trametinib-resistant AML cells treated with the trametinib-plus-idelalisib combination showed a pronounced decrease in viability compared with single-agent treatments. In contrast, JNKi, dasatinib, and palbociclib were able to overcome trametinib resistance as single agents (**Fig. 4C**). Further, the immunoblot analysis revealed that the decreased viability observed in trametinib-resistant AML cells was associated with the decreased activities of the PI3K/AKT, MAPK, SRC,

(*Continued.*) Red bars indicate increased activity for phosphokinases and blue bars indicate reduced activity relative to parental trametinib-sensitive MOLM13. **C,** Workflow of genome-wide CRISPR-Cas9 resensitization screen. Cas9 expressing MOLM13 trametinib-resistant cell line, cultured with CCL2, generated as described in **Fig. 2E** was transduced with the genome-wide CRISPR library. After puromycin selection, cells were treated with 100 nmol/L trametinib or DMSO for 14 days followed by DNA extraction and PCR amplification of the sgRNA barcodes. The resulting PCR library was subjected to NGS sequencing, and the data were analyzed for depleted and enriched sgRNA in trametinib-treated versus DMSO controls. **D,** Volcano plot of differential enrichment of sgRNA in trametinib-treated (100 nmol/L) versus DMSO-treated control AML cells, analyzed at day 14 of drug exposure. Mid log-fold change versus P values expressed as (−log10) are plotted with colors denoting the tiers associated with the ranking system for genes based on the statistically significant changes in guide numbers and guide/gene representation. **E,** Enrichment score plot for the MAPK1/3 signature that is significantly enriched in depleted sgRNA in trametinib-treated versus DMSO control **(F)** MOLM13 trametinib-resistant cells were transduced with sgRNA targeting *MAPK1/2, NRAS,* and *PIK3CD* genes and a nontargeting (NT) control. Viability was calculated using the indicated trametinib concentrations measured after 72 hours of treatment using an MTS assay. Representative of two independent experiments with consistent results using sgRNA to knockout each target gene. **G,** Pathways with altered protein levels downstream of CCL2 that can be combinatorically targeted with trametinib to mitigate AML cell survival and overcome trametinib resistance.

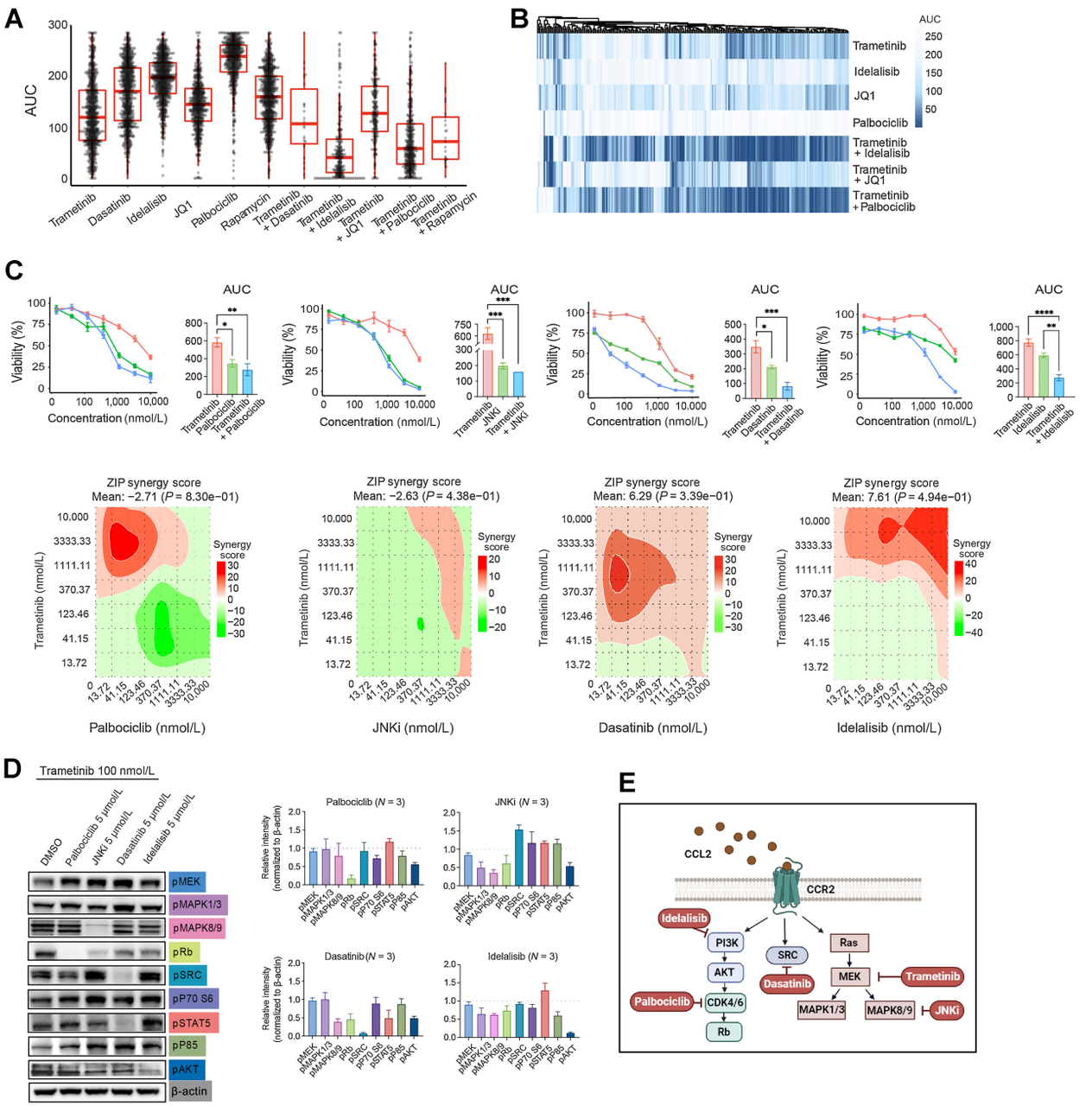

Figure. 4.

Targeting PI3K/AKT, MAPK, or cell-cycle pathways overcomes drug resistance mediated by CCL2. **A,** Boxplots with AUC values from *ex vivo* drug response curves for trametinib or the indicated agent alone and in combination with trametinib for indicated drugs for AML patient samples from the Beat AML dataset. **B,** Unsupervised clustering analyses of the data from **A**. **C,** Top: Comparisons of drug–response curves of MOLM13 trametinib-resistant cells treated with trametinib, tested as single agents or in combination with palbociclib, JNKi, dasatinib, and idelalisib with a dose gradient of 0.004 to 10 μmol/L, and their respective AUC. Statistical significance was determined using the one-way ANOVA. Bottom: Analyses of corresponding synergy matrix with red indicating synergistic action calculated using SynergyFinder. **D,** Immunoblot analysis of the trametinib-resistant MOLM13 cell line treated with trametinib (100 nmol/L) alone or in combination with palbociclib (5 μmol/L), JNKi (5 μmol/L), dasatinib (5 μmol/L), and idelalisib (5 μmol/L) as indicated. Relative band intensities from three independent experiments were measured with ImageJ, normalized to β-actin, and represented relative to DMSO-only treatment control, which is represented as a dashed line. **E,** Pathways targeted by specific small-molecule inhibitors used in **A–D**, in combination with trametinib, which were found activated in trametinib-resistant AML cells downstream of CCL2. *, $P \leq 0.05$; **, $P \leq 0.01$; ***, $P \leq 0.001$; ****, $P \leq 0.0001$.

and cell-cycle pathways. As anticipated with the second agent, combining trametinib with palbociclib decreased pRB and, separately, combining trametinib with a JNKi suppressed pJNK (pMAPK8/9), as well as pRB with slight changes in pAKT and pERK (pMAPK1/3). Additionally, combining trametinib with dasatinib suppressed pSRC, pRb, pSTAT5, pMAPK8/9, and pAKT, while combining trametinib with idelalisib decreased activity of pAKT and pMAPK8/9 (**Fig. 4D**). Taken together, these data revealed the downstream pathways elicited by CCL2 and demonstrated strategies to overcome trametinib resistance (**Fig. 4E**).

Targeting CCR2 suppresses AML cell proliferation and increases apoptosis in the presence of trametinib

To investigate the dependency of trametinib-resistant AML cells on the CCL2–CCR2 axis, we knocked down CCR2 in the MOLM13 trametinib-resistant cells using two independent shRNAs, which resulted in decreased viability (**Fig. 5A**). In a parallel approach, we targeted CCR2 using RS504393, a pharmacologic inhibitor of the receptor (58). Primary AML patient cells cultured with a dose gradient of trametinib and RS504393 showed lower IC_{50} and AUC values for the combination in comparison with the individual treatments (Supplementary Figs. S5A and S5B). Similarly, trametinib-resistant MOLM13 cells cultured in the presence of trametinib and RS504393 combination showed reduced viability compared with each single agent with 1.5-fold reduction in AUC (**Fig. 5B** and **C**), whereas trametinib-sensitive MOLM13 cells had no further improvement in sensitivity with the RS504393 and trametinib combination. Staining with cell trace violet to show a dilution of labeling in dividing cells revealed a reduction in cell proliferation at 48 hours for the combination treatment with trametinib and RS504393 in trametinib-resistant cells relative to untreated or single-agent-treated cells (**Fig. 5D** and **E**). In contrast, treatment of MOLM13 trametinib-sensitive cells showed decreased proliferation in both trametinib alone and combination treatments. Consistent with this finding, we observed increased apoptosis in the resistant cells upon combined treatment with trametinib and RS504393 on day 3 compared with single treatments (**Fig. 5F**; Supplementary Fig. S5C). These data demonstrate that targeting CCR2 resensitizes resistant AML cells to trametinib.

Finally, we assessed the downstream effects of inhibiting the CCL2/CCR2 signaling pathway in trametinib-resistant AML cells treated with trametinib and RS504393. Our results demonstrated that the combination treatment with trametinib and RS504393 efficiently reduced the levels of many downstream signaling including phospho-MEK, phospho-Rb, phospho-STAT5, and phospho-AKT as well as a trend toward a reduction for phospho-ERK1/2 (MAPK1/3), phospho-JNK1/2 (MAPK8/9), phospho-P85, and CCL2 (**Fig. 5G**).

Taken together, our findings demonstrate that increased CCL2-mediated signaling promotes drug resistance to MEK inhibition by the activation of several prosurvival pathways including PI3K/AKT, JNK, SRC, and CDK. Targeting each of these pathways in combination with trametinib or as a single agent can overcome the MEKi drug resistance in AML. We further suggest targeting the CCL2–CCR2 axis in combination with trametinib can be most effective in overcoming MEKi resistance in AML by suppressing multiple downstream signaling pathways at the same time.

Discussion

AML is a clonally heterogeneous disease with a poor prognosis. Despite initial efficacy, standard-of-care therapies often lead to the development of resistance, preventing complete remission and resulting in relapse (59). To address this challenge, combination therapy targeting multiple pathways involved in drug resistance is needed. For example, recent studies explored that the cotargeting of FLT3 mutations with extrinsic immune pathways such as IRAK1/4 may offer added benefits to overcome drug resistance, suggesting that combined targeting of intrinsic and extrinsic signaling might be beneficial (14, 60).

Therefore, we comprehensively evaluated 41 cytokines and correlated their levels with small-molecule inhibitor *ex vivo* sensitivity for approximately 300 AML patient samples. Our goal was to identify unique combinations of extrinsic and intrinsic signaling mechanisms that could overcome drug resistance in AML. We focused on MEKi resistance mechanisms, as clinical trials with MEK inhibition or MEK-AKT inhibition strategies in AML (NCT01907815) have achieved limited success (61), suggesting an improved understanding of mechanisms leading to refractory AML to MEKi is required. We showed that combined targeting of MEK and chemokine CCL2-driven signaling may lead to a novel combination strategy.

Dysregulation of the MAPK pathway, particularly the downstream MEK signaling, plays a significant role in AML pathogenesis. Mutations in the MAPK pathway, such as *NRAS, KRAS,* and *PTPN11*, lead to the constitutive activation of MEK signaling, promoting leukemic cell growth and survival (62). MEKi, such as trametinib, have shown potential for targeting aberrant MEK signaling in AML. However, resistance to MEKi poses a challenge (61), necessitating a deeper understanding.

Previously, various mechanisms have been proposed to explain the development of MEK resistance, including genetic alterations in the MAPK pathway, activation of alternative survival pathways, and remodeling in the tumor microenvironment (63, 64). We demonstrated that increased activation of the CCL2–CCR2 axis is associated with MEKi resistance by activating multiple prosurvival pathways. Further, these resistant cell lines maintained CCL2 levels even upon trametinib withdrawal, suggesting that CCL2 levels are also regulated by genetic, transcriptomic, or other molecular mechanisms, and a combination of these events promotes resistance in synergy with each other. Pharmacologic and genetic inhibition of the CCL2–CCR2 axis can overcome MEKi resistance by reducing cell proliferation and increasing apoptosis. Notably, CCL2 has been linked to drug resistance in solid tumors (65), and targeting CCL2/CCR2 with anti-CCL2/CCR2 or using *Ccr2*-deficient mice impedes the growth of tumor cells and improves survival (66). Unlike solid tumors, the involvement of CCL2/CCR2 axis in resistance to therapy is not fully explored in hematological malignancies. Our study establishes the applicability of targeting CCR2 signaling in drug-recalcitrant hematologic malignancies such as AML.

Previously, MEKi resistance has been observed in RAS-mutated leukemia (67), and RAS mutations are also acquired following FLT3i or BCL2i treatments (14, 68, 69). Combining MEK/AKT inhibitors has been suggested as a strategy to overcome MEKi resistance in leukemia (61, 70, 71). Similarly, cotargeting of the BCL2 and MEK pathways using venetoclax and cobimetinib can overcome venetoclax resistance (72). Our data indicate that targeting PI3K/AKT inhibition alone may not be sufficient to overcome MEKi resistance, as multiple prosurvival pathways associated with cell cycle, SRC, or MAPK signaling were activated by CCL2 but not inhibited by the combination of PI3K/AKT and trametinib. Therefore, exploring alternative combination therapies, such as CDK

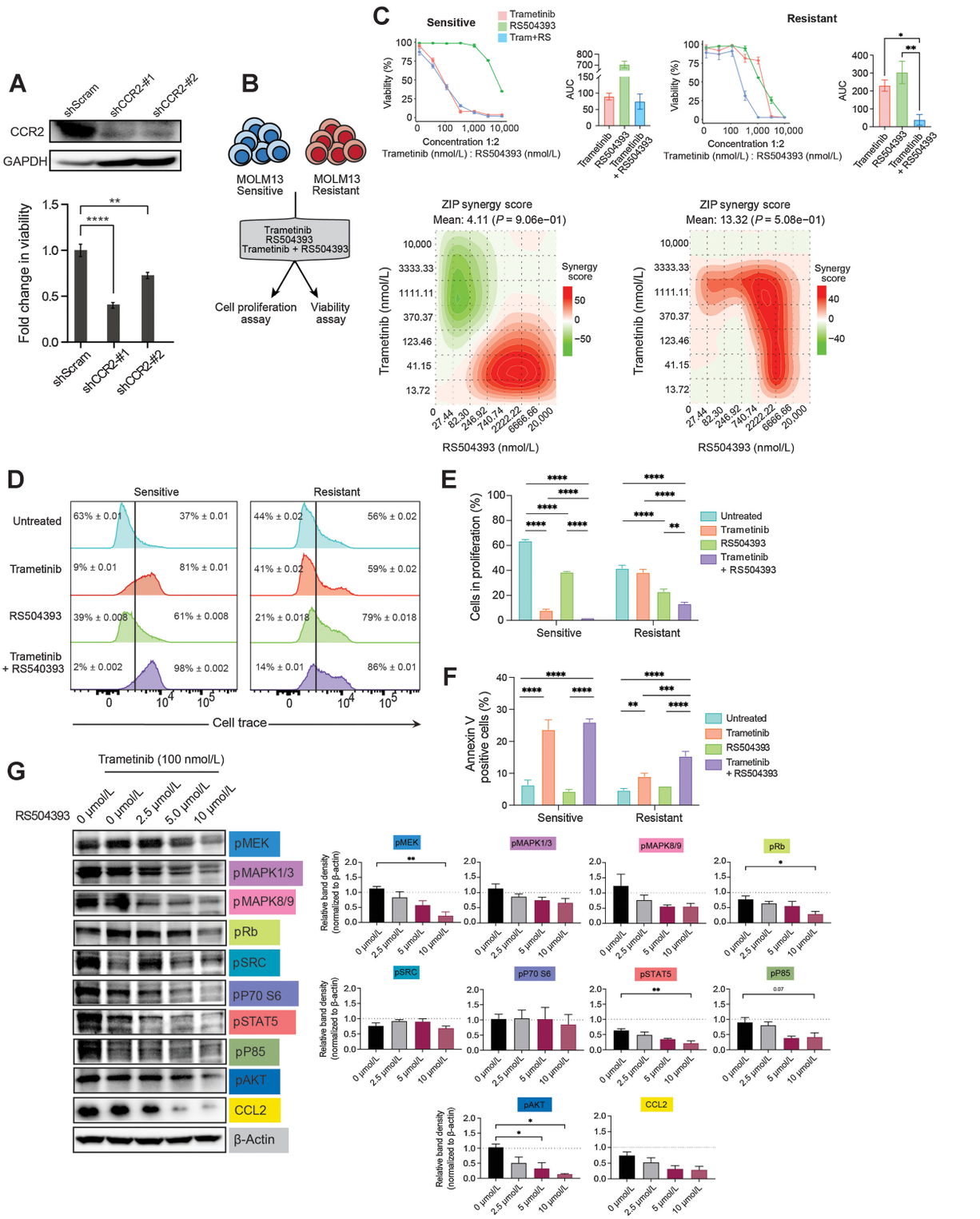

Figure. 5.

Targeting CCR2 in combination with trametinib reduced AML cell viability, cell proliferation, and induced apoptosis. **A,** Immunoblot analysis of CCR2 using trametinib-resistant MOLM13 cells expressing shRNAs for scrambled control and CCR2 (sh#1 and sh#2). GAPDH was used as a loading control (top). An equal number of cells was plated, and the viability of shRNA-transduced cells was determined by an MTS cell viability assay after 72 hours in culture. The data are represented as fold change over scrambled control shRNAs. (*Continued on the following page.*)

inhibitors, may be warranted for future clinical trials. Our data suggest that there is a positive feedback mechanism where upon trametinib exposure there is an increased secretion of CCL2 from AML cells and activation of multiple prosurvival pathways. These results further support the potential efficacy of direct CCR2 targeting to reduce CCL2 levels and enhance treatment response by inhibiting multiple downstream pathways together. In addition, targeting CCR2 signaling may improve traction in patients who fail to respond to MEKi due to emerging RAS mutations.

Importantly, our findings have implications beyond AML. Similar resistance mechanisms involving RAS mutations and MEK signaling have been observed in acute lymphoid leukemia (21) and solid tumors harboring activating mutations in the MAPK pathway, such as BRAF mutations in melanoma and KRAS mutations in colorectal cancer (73). Therefore, our study may contribute to addressing MEKi resistance in other leukemias and solid tumors.

In conclusion, our study reveals the involvement of the CCL2–CCR2 axis in MEKi resistance in AML. Our study highlights the potential of targeting CCR2 signaling as a promising strategy to overcome resistance and improve treatment outcomes. By evaluating the correlation between multiple cytokines and small-molecule inhibitors, we have generated valuable data for designing future combination therapies to suppress resistance development and prevent the emergence of resistant clones in AML and potentially other cancers.

Authors' Disclosures

K.G. De Oliveira Rebola reports grants from NIH during the conduct of the study. M.A. Gritsenko reports grants from NIH during the conduct of the study. P.D. Piehowski reports grants and nonfinancial support from NIH during the conduct of the study. D. Bottomly reports grants from NIH during the conduct of the study. K.D. Rodland reports grants from NCI during the conduct of the study. S.K. McWeeney reports grants from NIH during the conduct of the study. J.W. Tyner reports grants from Aptose, AstraZeneca, Constellation, Genentech, Incyte, Petra, Schrodinger, Meryx, Tolero, and Kronos and other support from Recludix outside the submitted work. A. Agarwal reports grants from NIH (ArtNet and CPTAC) during the conduct of the study. M. Mohammadhosseini and J. McClatchy report grants from NIH (NHLBI). No disclosures were reported by the other authors.

Authors' Contributions

R.V. Modak: Data curation, formal analysis, funding acquisition, validation, visualization, methodology, writing–original draft. **K.G. de Oliveira Rebola:** Formal analysis, validation, investigation, visualization, methodology, writing–original draft. **J. McClatchy:** Data curation, formal analysis, validation, investigation, visualization, methodology, writing–original draft, writing–review and editing. **M. Mohammadhosseini:** Data curation, formal analysis, validation, investigation, visualization, methodology, writing–original draft, writing–review and editing. **A. Damnernsawad:** Data curation, formal analysis, validation, investigation, visualization, methodology, writing–original draft, writing–review and editing. **S.E. Kurtz:** Data curation, formal analysis, visualization, methodology, writing–original draft. **C.A. Eide:** Data curation, formal analysis, visualization, writing–original draft. **G. Wu:** Data curation, formal analysis, validation, investigation, visualization, methodology, writing–original draft. **T. Laderas:** Data curation, formal analysis, investigation, visualization, methodology, writing–original draft. **T. Nechiporuk:** Data curation, formal analysis, validation, visualization, methodology, writing–original draft. **M.A. Gritsenko:** Data curation, formal analysis, investigation, methodology, writing–original draft. **J.R. Hansen:** Data curation, formal analysis, validation, investigation, methodology, writing–original draft. **C. Hutchinson:** Data curation, formal analysis, methodology, writing–original draft. **S.J. Gosline:** Data curation, formal analysis, funding acquisition, validation, investigation, visualization, writing–original draft. **P. Piehowski:** Resources, data curation, formal analysis, funding acquisition, investigation, methodology, writing–original draft. **D. Bottomly:** Data curation, visualization, methodology, writing–original draft. **N. Short:** Conceptualization, resources, investigation, methodology, writing–original draft. **K. Rodland:** Resources, funding acquisition, validation, investigation, writing–original draft. **S.K. McWeeney:** Resources, formal analysis, funding acquisition, validation, investigation, visualization, methodology, writing–original draft. **J.W. Tyner:** Resources, data curation, funding acquisition, validation, investigation, methodology, writing–original draft, writing–review and editing. **A. Agarwal:** Conceptualization, resources, data curation, formal analysis, supervision, funding acquisition, validation, investigation, visualization, methodology, writing–original draft, project administration, writing–review and editing.

Acknowledgments

We thank all of our patients at all sites for donating precious time and samples. DNA quality assessments, library creation, and short-read sequencing assays were conducted by the OHSU Massively Parallel Sequencing Shared Resource, with additional support provided by the Flow Cytometry Core. We thank Pranav Mandyam for his technical support. Funding for this project was provided by U54 CA224019 (to J.W. Tyner, S.K. McWeeney, A. Agarwal) and National Cancer Institute's Office of Cancer Clinical Proteomics Research [Clinical Proteomic Tumor Analysis Consortium (CPTAC)] under U01CA214116 (to J.W. Tyner and A. Agarwal) and U01CA271412 (to Paul Piehowski, J.W. Tyner, Sara J.C. Gosline, A. Agarwal), Tartar, and Medical Research Foundation funding (to R.V. Modak). A. Agarwal is also supported by grants from the NCI (R01 CA229875), National Heart, Lung, and Blood Institute (R01 HL155426), American Cancer Society (RSG-17–187–01-LIB), Alex Lemonade /Babich RUNX1 Foundation, Edward P. Evans Foundation, Chan Zuckerberg Initiative Funds, and V Foundation Scholar award. M. Mohammadhosseini and John McClatchy are supported by the National Heart, Lung, and Blood Institute NRSAF31 1F31HL162542 and 1F31HL164052, respectively. M. Mohammadhosseini was also funded through T32 (T32CA254888).

Note

Supplementary data for this article are available at Clinical Cancer Research Online (http://clincancerres.aacrjournals.org/).

Received September 2, 2023; revised December 29, 2023; accepted March 5, 2024; published first March 7, 2024.

(*Continued.*) Statistical significance was determined via the two-way ANOVA. **B,** The cell proliferation and viability assays performed with MOLM13 trametinib-resistant and sensitive cell lines. **C,** Drug–response curve of trametinib-sensitive (S) and -resistant (R) MOLM13 cells treated with trametinib (0.004–10 μmol/L) and RS540393 (0.008–20 μmol/L) for 7 days, as determined using the MTS cell viability assay. Significance was calculated using one-way ANOVA with multiple comparisons, where $P \leq 0.05$ was considered significant. **D,** Representative flow cytometry histograms showing levels of cell trace violet in the sensitive and trametinib-resistant MOLM13 cell lines after 48 hours of treatment with either 100 nmol/L trametinib or 2.5 μmol/L RS504393, or their combination. **E,** Bar graphs of data in **D**, representing the percentage of proliferating cells compared with untreated control in respective cell lines. Data are plotted as mean ± SEM. Significance as calculated using the two-way ANOVA. The data are representative of three independent experiments. **F,** Representative plots of Annexin V and 7-AAD staining from trametinib-sensitive (S) and -resistant (R) MOLM13 cells treated with 100 nmol/L trametinib or 2.5 μmol/L RS504393 or a combination of both for 72 hours. Significance was calculated using the two-way ANOVA. The data are representative of three independent experiments. **G,** Immunoblot analysis of the trametinib-resistant line treated with trametinib (100 nmol/L) in combination with RS504393 across the indicated concentrations (left). Relative band densities of immunoblots (right) were measured using ImageJ, normalized to β-actin and represented relative to DMSO-only treatment control, which is shown as a dashed line. *, $P \leq 0.05$; **, $P \leq 0.01$; ***, $P \leq 0.001$; ****, $P \leq 0.0001$.

References

1. 2018 National Cancer Institute: Surveillance, Epidemiology, and End Results Program. Available from: https://seer.cancer.gov/statfacts/.
2. Jemal A, Siegel R, Xu J, Ward E. Cancer statistics 2010. CA Cancer J Clin 2010;60: 277–300.
3. Papaemmanuil E, Gerstung M, Bullinger L, Gaidzik VI, Paschka P, Roberts ND, et al. Genomic classification and prognosis in acute myeloid leukemia. N Engl J Med 2016;374:2209–21.
4. TCGA. Genomic and epigenomic landscapes of adult de novo acute myeloid leukemia. N Engl J Med 2013;368:2059–74.
5. Tyner JW, Tognon CE, Bottomly D, Wilmot B, Kurtz SE, Savage SL, et al. Functional genomic landscape of acute myeloid leukaemia. Nature 2018;562: 526–31.
6. Rohle D, Popovici-Muller J, Palaskas N, Turcan S, Grommes C, Campos C, et al. An inhibitor of mutant IDH1 delays growth and promotes differentiation of glioma cells. Science 2013;340:626–30.
7. Stone RM, Mandrekar SJ, Sanford BL, Laumann K, Geyer S, Bloomfield CD, et al. Midostaurin plus chemotherapy for acute myeloid leukemia with a FLT3 mutation. N Engl J Med 2017;377:454–64.
8. Wang F, Travins J, DeLaBarre B, Penard-Lacronique V, Schalm S, Hansen E, et al. Targeted inhibition of mutant IDH2 in leukemia cells induces cellular differentiation. Science 2013;340:622–6.
9. Short NJ, Konopleva M, Kadia TM, Borthakur G, Ravandi F, DiNardo CD, et al. Advances in the treatment of acute myeloid leukemia: new drugs and new challenges. Cancer Discov 2020;10:506–25.
10. DiNardo CD, Pratz K, Pullarkat V, Jonas BA, Arellano M, Becker PS, et al. Venetoclax combined with decitabine or azacitidine in treatment-naive, elderly patients with acute myeloid leukemia. Blood 2019;133:7–17.
11. Puthier D, Derenne S, Barille S, Moreau P, Harousseau JL, Bataille R, et al. Mcl-1 and Bcl-xL are co-regulated by IL-6 in human myeloma cells. Br J Haematol 1999;107:392–5.
12. Zeng Z, Shi YX, Samudio IJ, Wang RY, Ling X, Frolova O, et al. Targeting the leukemia microenvironment by CXCR4 inhibition overcomes resistance to kinase inhibitors and chemotherapy in AML. Blood 2009;113: 6215–24.
13. Meads MB, Hazlehurst LA, Dalton WS. The bone marrow microenvironment as a tumor sanctuary and contributor to drug resistance. Clin Cancer Res 2008;14: 2519–26.
14. Joshi SK, Nechiporuk T, Bottomly D, Piehowski PD, Reisz JA, Pittsenbarger J, et al. The AML microenvironment catalyzes a stepwise evolution to gilteritinib resistance. Cancer Cell 2021;39:999–1014.
15. Traer E, Martinez J, Javidi-Sharifi N, Agarwal A, Dunlap J, English I, et al. FGF2 from marrow microenvironment promotes resistance to FLT3 inhibitors in acute myeloid leukemia. Cancer Res 2016;76:6471–82.
16. Carey A, Edwards DK 5th, Eide CA, Newell L, Traer E, Medeiros BC, et al. Identification of Interleukin-1 by functional screening as a key mediator of cellular expansion and disease progression in acute myeloid leukemia. Cell Rep 2017;18:3204–18.
17. Hosseini MM, Kurtz SE, Abdelhamed S, Mahmood S, Davare MA, Kaempf A, et al. Inhibition of interleukin-1 receptor-associated kinase-1 is a therapeutic strategy for acute myeloid leukemia subtypes. Leukemia 2018;32:2374–87.
18. Arranz L, Arriero MDM, Villatoro A. Interleukin-1beta as emerging therapeutic target in hematological malignancies and potentially in their complications. Blood Rev 2017;31:306–17.
19. Turzanski J, Grundy M, Russell NH, Pallis M. Interleukin-1beta maintains an apoptosis-resistant phenotype in the blast cells of acute myeloid leukaemia via multiple pathways. Leukemia 2004;18:1662–70.
20. Borthakur G, Popplewell L, Boyiadzis M, Foran J, Platzbecker U, Vey N, et al. Activity of the oral mitogen-activated protein kinase kinase inhibitor trametinib in RAS-mutant relapsed or refractory myeloid malignancies. Cancer 2016;122: 1871–9.
21. Knight T, Irving JA. Ras/Raf/MEK/ERK pathway activation in childhood acute lymphoblastic leukemia and its therapeutic targeting. Front Oncol 2014;4:160.
22. Smith AM, Zhang CRC, Cristino AS, Grady JP, Fink JL, Moore AS, et al. PTEN deletion drives acute myeloid leukemia resistance to MEK inhibitors. Oncotarget 2019;10:5755–67.
23. Dutta P, Sarkissyan M, Paico K, Wu Y, Vadgama JV. MCP-1 is overexpressed in triple-negative breast cancers and drives cancer invasiveness and metastasis. Breast Cancer Res Treat 2018;170:477–86.
24. Sun X, Glynn DJ, Hodson LJ, Huo C, Britt K, Thompson EW, et al. CCL2-driven inflammation increases mammary gland stromal density and cancer susceptibility in a transgenic mouse model. Breast Cancer Res 2017;19:4.
25. Kitamura T, Qian BZ, Soong D, Cassetta L, Noy R, Sugano G, et al. CCL2-induced chemokine cascade promotes breast cancer metastasis by enhancing retention of metastasis-associated macrophages. J Exp Med 2015;212:1043–59.
26. Jin J, Lin J, Xu A, Lou J, Qian C, Li X, et al. CCL2: an important mediator between tumor cells and host cells in tumor microenvironment. Front Oncol 2021;11: 722916.
27. Kalbasi A, Komar C, Tooker GM, Liu M, Lee JW, Gladney WL, et al. Tumor-derived CCL2 mediates resistance to radiotherapy in pancreatic ductal adenocarcinoma. Clin Cancer Res 2017;23:137–48.
28. Zhang J, Lu Y, Pienta KJ. Multiple roles of chemokine (C-C motif) ligand 2 in promoting prostate cancer growth. J Natl Cancer Inst 2010;102:522–8.
29. Eisenkraft A, Keidan I, Bielorai B, Keller N, Toren A, Paret G. MCP-1 in the cerebrospinal fluid of children with acute lymphoblastic leukemia. Leuk Res 2006;30:1259–61.
30. Ritchie ME, Phipson B, Wu D, Hu Y, Law CW, Shi W, et al. limma powers differential expression analyses for RNA-sequencing and microarray studies. Nucleic Acids Res 2015;43:e47.
31. Merico D, Isserlin R, Stueker O, Emili A, Bader GD. Enrichment map: a network-based method for gene-set enrichment visualization and interpretation. PLoS One 2010;5:e13984.
32. Yang F, Long N, Anekpuritanang T, Bottomly D, Savage JC, Lee T, et al. Identification and prioritization of myeloid malignancy germline variants in a large cohort of adult patients with AML. Blood 2022;139:1208–21.
33. Tyner JW, Yang WF, Bankhead A 3rd, Fan G, Fletcher LB, Bryant J, et al. Kinase pathway dependence in primary human leukemias determined by rapid inhibitor screening. Cancer Res 2013;73:285–96.
34. Ianevski A, Giri AK, Aittokallio T. SynergyFinder 3.0: an interactive analysis and consensus interpretation of multi-drug synergies across multiple samples. Nucleic Acids Res 2022;50(W1):W739–W43.
35. Mertins P, Tang LC, Krug K, Clark DJ, Gritsenko MA, Chen L, et al. Reproducible workflow for multiplexed deep-scale proteome and phosphoproteome analysis of tumor tissues by liquid chromatography-mass spectrometry. Nat Protoc 2018; 13:1632–61.
36. Tsai CF, Wang YT, Hsu CC, Kitata RB, Chu RK, Velickovic M, et al. A streamlined tandem tip-based workflow for sensitive nanoscale phosphoproteomics. Commun Biol 2023;6:70.
37. Tsai CF, Zhao R, Williams SM, Moore RJ, Schultz K, Chrisler WB, et al. An improved boosting to amplify signal with isobaric labeling (iBASIL) strategy for precise quantitative single-cell proteomics. Mol Cell Proteomics 2020;19: 828–38.
38. Beausoleil SA, Villen J, Gerber SA, Rush J, Gygi SP. A probability-based approach for high-throughput protein phosphorylation analysis and site localization. Nat Biotechnol 2006;24:1285–92.
39. Tzelepis K, Koike-Yusa H, De Braekeleer E, Li Y, Metzakopian E, Dovey OM, et al. A CRISPR dropout screen identifies genetic vulnerabilities and therapeutic targets in acute myeloid leukemia. Cell Rep 2016;17:1193–205.
40. Nechiporuk T, Kurtz SE, Nikolova O, Liu T, Jones CL, D'Alessandro A, et al. The TP53 apoptotic network is a primary mediator of resistance to BCL2 inhibition in AML cells. Cancer Discov 2019;9:910–25.
41. Shalem O, Sanjana NE, Hartenian E, Shi X, Scott DA, Mikkelson T, et al. Genome-scale CRISPR-Cas9 knockout screening in human cells. Science 2014; 343:84–7.
42. Martin M. Cutadapt removes adapter sequences from high-throughput sequencing reads. EMBnetjournal 2011. Doi:1014806/ej171200
43. Langmead B, Salzberg SL. Fast gapped-read alignment with Bowtie 2. Nat Methods 2012;9:357–9.
44. Barnett DW, Garrison EK, Quinlan AR, Stromberg MP, Marth GT. BamTools: a C++ API and toolkit for analyzing and managing BAM files. Bioinformatics 2011;27:1691–2.
45. Robinson MD, Oshlack A. A scaling normalization method for differential expression analysis of RNA-seq data. Genome Biol 2010;11:R25.
46. Robinson MD, McCarthy DJ, Smyth GK. edgeR: a bioconductor package for differential expression analysis of digital gene expression data. Bioinformatics 2010;26:139–40.
47. Storey J. The positive false discovery rate: a Bayesian interpretation and the q-value. Ann Statist 2003;31:2013–35.

48. Wu D, Smyth GK. Camera: a competitive gene set test accounting for inter-gene correlation. Nucleic Acids Res 2012;40:e133.
49. Mazur G, Wrobel T, Butrym A, Kapelko-Slowik K, Poreba R, Kuliczkowski K. Increased monocyte chemoattractant protein 1 (MCP-1/CCL-2) serum level in acute myeloid leukemia. Neoplasma 2007;54:285–9.
50. Macanas-Pirard P, Quezada T, Navarrete L, Broekhuizen R, Leisewitz A, Nervi B, et al. The CCL2/CCR2 axis affects transmigration and proliferation but not resistance to chemotherapy of acute myeloid leukemia cells. PLoS One 2017;12: e0168888.
51. Gschwandtner M, Derler R, Midwood KS. More than just attractive: how CCL2 influences myeloid cell behavior beyond chemotaxis. Front Immunol 2019;10: 2759.
52. Arefieva TI, Kukhtina NB, Antonova OA, Krasnikova TL. MCP-1-stimulated chemotaxis of monocytic and endothelial cells is dependent on activation of different signaling cascades. Cytokine 2005;31:439–46.
53. Cambien B, Pomeranz M, Millet MA, Rossi B, Schmid-Alliana A. Signal transduction involved in MCP-1-mediated monocytic transendothelial migration. Blood 2001;97:359–66.
54. Damnernsawad A, Eide C, Beer A, Zhang H, Bottomly D, Kurtz S, et al. Characterization of trametinib combined with venetoclax in acute myeloid leukemia (AML) treatment. Cancer Res 2021;81 (13_Supplement): Abstract 1429.
55. Casado P, Rodriguez-Prados JC, Cosulich SC, Guichard S, Vanhaesebroeck B, Joel S, et al. Kinase-substrate enrichment analysis provides insights into the heterogeneity of signaling pathway activation in leukemia cells. Sci Signal 2013;6: rs6.
56. Wiredja DD, Koyuturk M, Chance MR. The KSEA app: a web-based tool for kinase activity inference from quantitative phosphoproteomics. Bioinformatics 2017;33:3489–91.
57. Tonini C, Colardo M, Colella B, Di Bartolomeo S, Berardinelli F, Caretti G, et al. Inhibition of bromodomain and extraterminal domain (BET) proteins by JQ1 unravels a novel epigenetic modulation to control lipid homeostasis. Int J Mol Sci 2020;21:1297.
58. Mirzadegan T, Diehl F, Ebi B, Bhakta S, Polsky I, McCarley D, et al. Identification of the binding site for a novel class of CCR2b chemokine receptor antagonists: binding to a common chemokine receptor motif within the helical bundle. J Biol Chem 2000;275:25562–71.
59. Short NJ, Ravandi F. How close are we to incorporating measurable residual disease into clinical practice for acute myeloid leukemia? Haematologica 2019; 104:1532–41.
60. Melgar K, Walker MM, Jones LM, Bolanos LC, Hueneman K, Wunderlich M, et al. Overcoming adaptive therapy resistance in AML by targeting immune response pathways. Sci Transl Med 2019;11:eaaw8828.
61. Ragon BK, Odenike O, Baer MR, Stock W, Borthakur G, Patel K, et al. Oral MEK 1/2 inhibitor trametinib in combination with AKT inhibitor GSK2141795 in patients with acute myeloid leukemia with RAS mutations: a phase II study. Clin Lymphoma Myeloma Leuk 2019;19:431–40.
62. Desikan SP, Ravandi F, Pemmaraju N, Konopleva M, Loghavi S, Jabbour EJ, et al. A phase II study of azacitidine, venetoclax, and trametinib in relapsed or refractory acute myeloid leukemia harboring RAS pathway-activating mutations. Acta Haematol 2022;145:529–36.
63. Farnsworth DA, Inoue Y, Johnson FD, de Rappard-Yuswack G, Lu D, Shi R, et al. MEK inhibitor resistance in lung adenocarcinoma is associated with addiction to sustained ERK suppression. NPJ Precision Oncology 2022;6:88.
64. Kun E, Tsang YTM, Ng CW, Gershenson DM, Wong KK. MEK inhibitor resistance mechanisms and recent developments in combination trials. Cancer Treat Rev 2021;92:102137.
65. Qian DZ, Rademacher BL, Pittsenbarger J, Huang CY, Myrthue A, Higano CS, et al. CCL2 is induced by chemotherapy and protects prostate cancer cells from docetaxel-induced cytotoxicity. Prostate 2010;70:433–42.
66. Felsenstein M, Blank A, Bungert AD, Mueller A, Ghori A, Kremenetskaia I, et al. CCR2 of tumor microenvironmental cells is a relevant modulator of glioma biology. Cancers (Basel) 2020;12:1882.
67. Steelman LS, Franklin RA, Abrams SL, Chappell W, Kempf CR, Basecke J, et al. Roles of the Ras/Raf/MEK/ERK pathway in leukemia therapy. Leukemia 2011; 25:1080–94.
68. McMahon CM, Ferng T, Canaani J, Wang ES, Morrissette JJD, Eastburn DJ, et al. Clonal selection with RAS pathway activation mediates secondary clinical resistance to selective FLT3 inhibition in acute myeloid leukemia. Cancer Discov 2019;9:1050–63.
69. Zhang Q, Riley-Gillis B, Han L, Jia Y, Lodi A, Zhang H, et al. Activation of RAS/MAPK pathway confers MCL-1 mediated acquired resistance to BCL-2 inhibitor venetoclax in acute myeloid leukemia. Signal Transduct Target Ther 2022;7:51.
70. Dumble M, Crouthamel MC, Zhang SY, Schaber M, Levy D, Robell K, et al. Discovery of novel AKT inhibitors with enhanced anti-tumor effects in combination with the MEK inhibitor. PLoS One 2014;9:e100880.
71. Hofmann I, Weiss A, Elain G, Schwaederle M, Sterker D, Romanet V, et al. K-RAS mutant pancreatic tumors show higher sensitivity to MEK than to PI3K inhibition in vivo. PLoS One 2012;7:e44146.
72. Han L, Zhang Q, Dail M, Shi C, Cavazos A, Ruvolo VR, et al. Concomitant targeting of BCL2 with venetoclax and MAPK signaling with cobimetinib in acute myeloid leukemia models. Haematologica 2020;105:697–707.
73. Grimaldi AM, Simeone E, Festino L, Vanella V, Strudel M, Ascierto PA. MEK inhibitors in the treatment of metastatic melanoma and solid tumors. Am J Clin Dermatol 2017;18:745–54.